Replicated mask surface roughness effects on EUV lithographic patterning and line edge roughness

Simi A. George*, Patrick P. Naulleau, Eric M. Gullikson, Iacopo Mochi, Farhad Salmassi, Kenneth A. Goldberg and Erik H. Anderson

Center for X-Ray Optics, Lawrence Berkeley National Laboratory, Berkeley, California 94720
*Now at SCHOTT North America, Duryea, PA 18642

Email: *simi.george@us.schott.com* and *pnaulleau@lbl.gov*

ABSTRACT

To quantify the roughness contributions to speckle, a programmed roughness substrate was fabricated with a number of areas having different roughness magnitudes. The substrate was then multilayer coated. Atomic force microscopy (AFM) surface maps were collected before and after multilayer deposition. At-wavelength reflectance and total integrated scattering measurements were also completed. Angle resolved scattering based power spectral densities are directly compared to the AFM based power spectra. We show that AFM overpredicts the roughness in the picometer measurements range. The mask was then imaged at-wavelength for the direct characterization of the aerial image speckle using the SEMATECH Berkeley Actinic Inspection Tool (AIT). Modeling was used to test the effectiveness of the different metrologies in predicting the measured aerial-image speckle. AIT measured contrast values are 25% or more than the calculated image contrast values obtained using the measured rms roughness input. The extent to which the various metrologies can be utilized for specifying tolerable roughness limits on EUV masks is still to be determined. Further modeling and measurements are being planned.

Keywords: extreme ultraviolet, EUV mask, phase roughness, replicated surface roughness, speckle, actinic inspection, scattering, multilayer reflectivity

1. INTRODUCTION

The International Technology Roadmap for Semiconductors (ITRS) has set the current limit on line edge roughness (LER) in resists to be less than 1.2 nm (3σ LER) at 20 nm half-pitch resolution. With such extreme limits, it is expected that mask contributors to LER may play a significant role. For extreme ultraviolet (EUV) masks, there is particular concern about scattering leading to image plane speckle. Correlated scattering that comes from phase coherent substrate roughness that propagates conformally from layer to layer, termed replicated surface roughness (RSR), is the most important since it leads to random phase errors at the mask. Uncorrelated scattering from the roughness at the different interfaces of the multilayer structures, on the other hand, is of less concern, but still needs to be taken into account since it can lead to fine-scale reflectivity variations across the mask. In recent years, modeling studies have shown that RSR must be limited to 50 picometers to meet current LER targets for the 22 and 16-nm half-pitch lithography nodes [1].

For EUV masks and optics' multilayer (ML) characterization, top-surface roughness analysis methods such as Atomic Force Microscopy (AFM) are typically used. AFM, however, only characterizes the top surface relief structure, making the roughness evaluation for scattering based on such measurements more qualitative than quantitative. Information buried within the multilayer structures, such as RSR, defects and interfacial effects, are neglected when only the top surface profiles are considered.

For this paper, we attempt to quantify the roughness contributions to speckle by measuring a mask with multilayer areas programmed to have spatially varying substrate roughness magnitudes. With AFM surface maps collected before and

after multilayer deposition, we are able to isolate the impact of substrate roughness on the final image plane. At-wavelength reflectance and total integrated scattering measurements are completed on all of the multilayers on the mask to make a direct comparison to the AFM roughness measurements. Finally, this mask is imaged at-wavelength for the direct characterization of the aerial image speckle using the SEMATECH Berkeley Actinic Inspection Tool (AIT) [2-4]. Furthermore, modeling is used to test the effectiveness of the different metrologies in predicting the measured aerial-image speckle. Through this exercise, we are able to quantify the extent to which the various metrologies can be utilized for specifying tolerable roughness limits on EUV masks.

2. PROGRAMMED ROUGHNESS CONTENT AND MEASUREMENTS

An overview of the mask fabrication procedures for generating reflective surfaces with different roughness content is described here. Surface profiles are collected using an AFM and scattering measurements on each of the multilayer surfaces are completed at wavelength.

2.1 A mask with multilayer areas containing different substrate roughness content

Typically, substrates with different surface polishes are used to evaluate the impact of roughness on image plane. Since this method is time consuming and not economical, a single mask surface with a surface roughness gradient was created at the nanofabrication and multilayer coating facilities of the Center for X-Ray Optics [5]. The fabrication procedure involved the shadowed deposition of Chromium (Cr) onto a standard 4-inch Silicon (Si) wafer. The deposition was completed using DC magnetron sputtering in an Argon gas environment. The shadowing was controlled to produce a thickness gradient from 0.2 nm to 1.4 nm, along one direction on the wafer. Since surface roughness is a function of film thickness, a roughness gradient of 0.25 nm to 0.75 nm root mean squared (rms) was achieved as measured over a 5 x 5 μm area using a Digital Instruments model DM 3100 AFM.

A typical EUV Molybdenum (Mo) and Si multilayer (40 alternating pairs of Si and Mo films such that each pair is 7 nm in thickness totaling approximately 240 nm) designed for near-normal reflection was deposited on top of the sputter-coated Cr surface of the wafer. Peak reflectivity for this multilayer was measured to be at 13.46 nm wavelength. To define the measurement regions, an e-beam resist was used as the absorber; the resist was spun-coated onto the multilayer surface with a thickness about 380 nm, 760 nm round trip for full attenuation of EUV light. A grid of windows sized 1 x 3 mm and separated by 1.5 mm was patterned to expose the multilayer surface. A second set of AFM images was collected from the exposed multilayer surface at roughly the same positions as the AFM measurements on the bare substrate completed previously. For the metrologies completed here, we look at a row of 18 windows ranging from low roughness to high roughness as shown in figure 1.

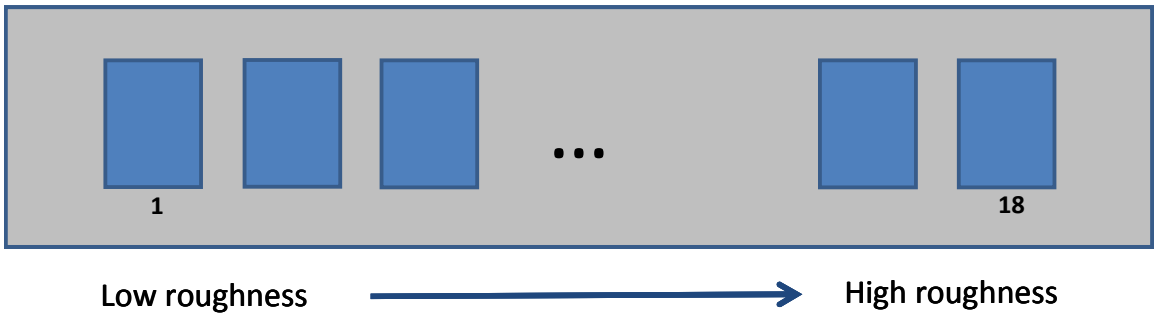

Figure 1: A grid pattern of windows sized 1 x 3 mm and separated by 1.5 mm, revealing regions from low substrate roughness to high roughness. There are a total of 18 windows sized 1 x 3 mm and separated by 1.5 mm in the row that was evaluated for this study. The clear multilayer surface is inside the window and resist absorber giving full attenuation of EUV is on the outside.

2.2 AFM measurements

The rms roughness computed from AFM images collected before and after multilayer is plotted in figure 2. The rms values are plotted as a function of increasing region number (correlated to the increase in the chromium thickness and

roughness). After ML deposition, the minimum measured roughness is 0.2 nm which gives approximately 1.9 nm peak-valley (p-v) errors. The maximum roughness is 0.54 nm and corresponds to nearly 5 nm of p-v errors. We attribute the flattening of the curve to multilayer smoothing occurring in the rougher mask areas after ML deposition. On the other hand, very little smoothing is observed at the smaller substrate roughness regions near 0.2 nm, which is concluded to be the result of the ML itself having intrinsic roughness. The characteristic correlation lengths computed from the autocorrelation of the image surface heights is found to be on the order of 60 nm, on average.

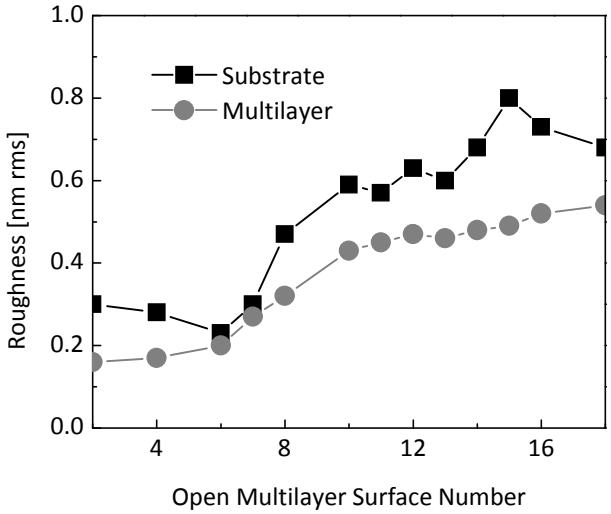

Figure 2: Root mean square height deviations from the AFM surface profiles measured before and after Mo/Si multilayer coating. Rougher areas of the mask show smoothing after multilayer is deposited and at smaller roughness scales, the smoothing appears to be diminished.

Figure 3 shows the roughness power spectral densities (PSD) from the images collected before and after ML depositions, compared at a roughness minimum and roughness maximum values. The measured minimum roughness is 0.23 nm before ML coating and 0.2 nm after. The roughest area on the mask shows a reduction from 0.8 nm to 0.5 nm rms roughness after the ML is deposited. In comparing the PSDs generated for the (figure 3, left) low roughness region, we see some smoothing in the mid spatial frequencies and enhanced roughness at the highest spatial frequencies after ML coating. In contrast, the PSDs for the region with taller phase structures show significant reduction into all frequencies after ML deposition. This effect is concluded to be due to the smoothing resulting from the thin film deposition.

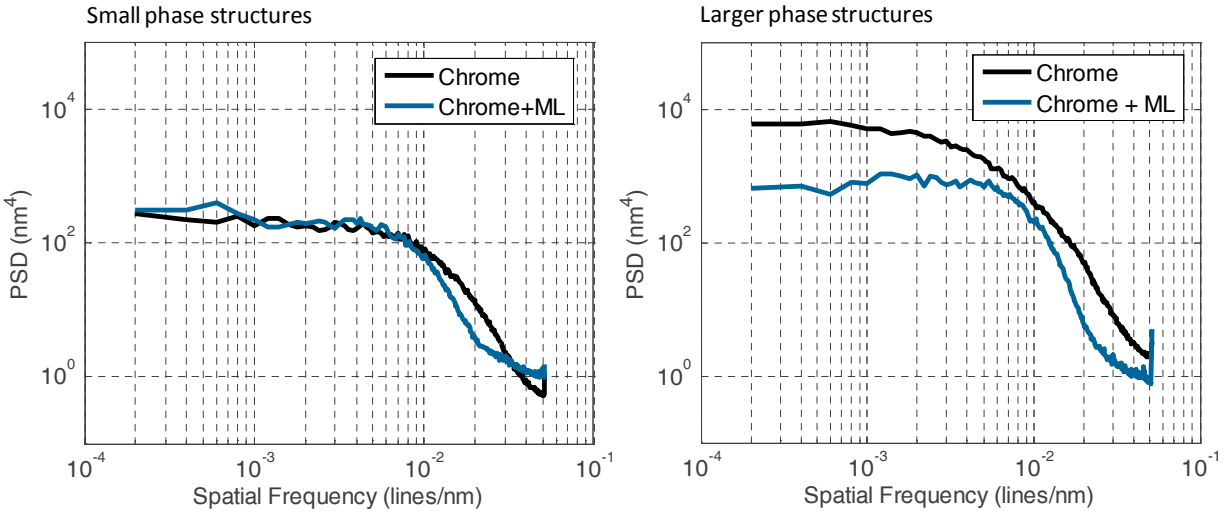

Figure 3: PSDs generated in the low roughness region (left) with the solid black curve is the PSD of the Chromium surface by itself. An increase in the low spatial frequency range (LSFR) and some smoothing into the mid to high spatial frequencies (MSFR and HSFR) are observed after the ML is coated on this surface. In contrast, the PSDs for high roughness (right) show significant reduction into all frequencies after ML deposition. The taller phase structures are assumed to have been smoothed.

2.3 Reflectivity and scattering measurements at fixed wavelength

Scattering measurements made at the wavelength of peak reflectivity are typically used to study roughness related effects from within a multilayer. X-ray reflectivity and scattering (XRS) measurements at wavelength were made on the rough multilayer surfaces using the synchrotron-based reflectometer of the Calibrations and Standards Beamline 6.3.2 located at the Advanced Light Source (ALS), Lawrence Berkeley National Laboratory (LBNL). The main advantage of this beamline is its high spectral purity, a spectral resolving power ($E/\Delta E$) of up to 7000, a wavelength accuracy of 10^{-3} nm, and a reflectivity accuracy of 0.1% (absolute) [6]. Reflectance measurements were performed at a wavelength of 13.46 nm with a relative spectral bandwidth, $\Delta\lambda/\lambda$, of approximately 0.01%. The photon beam is incident on the sample surface at a 5° angle from normal. The specular beam divergence is ±1.2° and the detector is large in comparison to reflected beam.

Diffuse scattering from the surfaces is measured at a fixed 5° angle from the reflected beam or 10° away from the surface normal. The raw reflectivity and scattering yields for the measurements from the different windows are shown in figure 4 on a scale of increasing roughness. Scattering measurements are obtained at a single spatial frequency and serve to illustrate that an increase in phase roughness scatters intensity away from reflected specular beam. In figure 4, the increase in scattering is seen to follow the decrease in reflectivity owing to the increase in phase roughness of the measured surfaces.

2.4 Angle resolved scattering at wavelength

Measurements of the angular distribution of the scattering were also made using the reflectometer. Apertures upstream of the reflectometer end-station block any scattering from the beamline optics, and measurements were performed with s-polarized radiation. A channel electron multiplier (CEM) is used for the scattering measurements; a scattering angle of zero is assigned at the multilayer normal, where the strongest scattering is observed. To measure scattered intensities on an absolute scale, the incident intensity was measured with a GaAsP photodiode and the efficiency of the CEM was measured relative to the photodiode using an intensity where both detectors could be used. The detection efficiency of the CEM was approximately 5% for the wavelength of interest. A 2-mm-diameter circular aperture in front of the detectors (positioned 225 mm away from the sample) limits the angular resolution to 0.5°, and the solid angle collected was $6.2\text{x}10^{-5}$ steradian. The angular range of 1–30° was studied, and measurements were made in each window-defined region, giving 18 angle resolved scatter spectra. A sample of the data obtained with this measurement is given in figure 5.

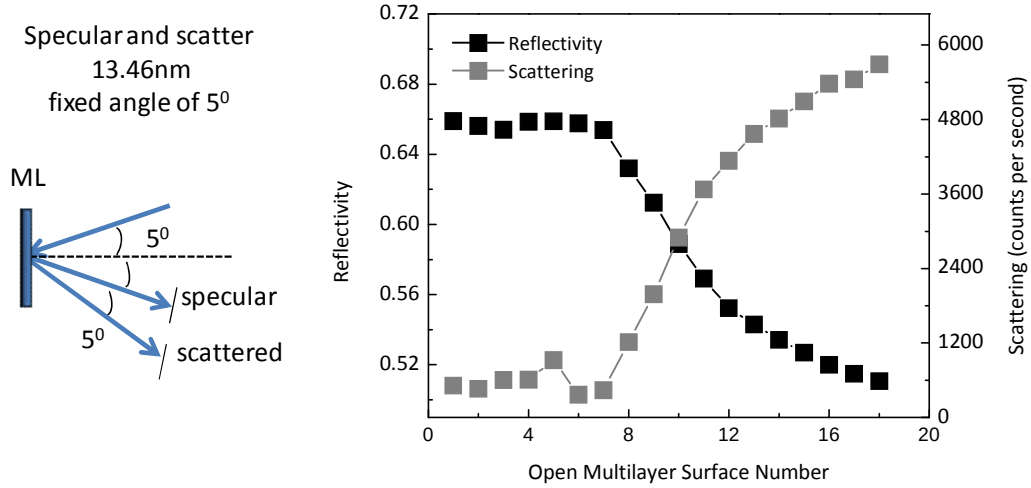

Figure 4: The reflectivity and scattering yields for the measurements from the different windows are shown on the scale of increasing roughness. An increase in scattering follows the decrease in reflectivity, indicating greater phase roughness. The wavelength of light used was 13.46 nm at a 5° angle of incidence. The scattered intensity was measured at a fixed angle 10° from normal.

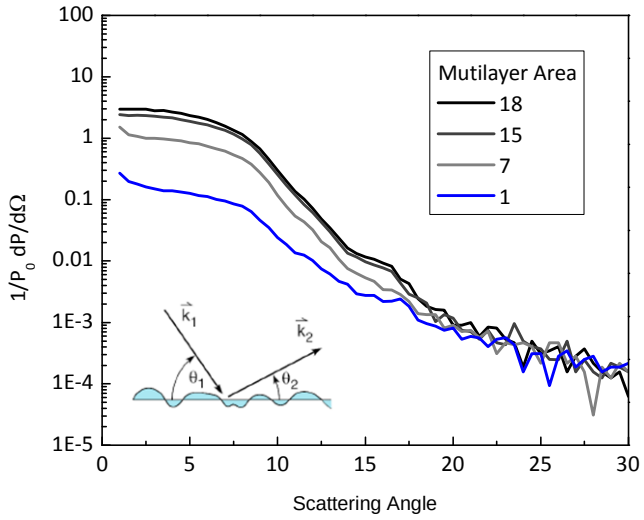

Figure 5: Angle resolved scattering measurements obtained for the rough mask multilayer surfaces. Only a few of the 18 multilayer regions measured are shown. The curves illustrate increase in scattering intensities as a function of roughness of the substrate. The measurements are computed on an absolute scale. Mutilayer region 1 is the lowest roughness content, and 18 has the highest roughness content and produces the most scatter (top most curve).

3. COMPARING 2D MEASUREMENTS TO SCATTERING AT WAVELENGTH

For approximating roughness from the fixed angle scatter measurements, we use the Debye-Waller factor for the relationship between the reduction of reflectivity and the total integrated scatter (TIS),

$$TIS = \left(\frac{4\pi\sigma \cos\theta}{\lambda} \right)^2 = 1 - \frac{R}{R_0} \qquad \text{Eq. (1)}$$

where σ and is the rms phase roughness, λ is the illuminating wavelength at the given angle of incidence, θ. R_0 and R denote the reflectivity of the best surface and the reflectivity of the surfaces with increasing roughness content, respectively. Total reflectivity is reduced because amplitudes reflected from different depths add with different phases.

From the angle resolved scattering measurements, the rms roughness of the multilayer can be calculated by integrating over the scattering hemisphere and relating it to the expression for the TIS from a single surface,

$$TIS = \frac{1}{P_0} \int \frac{dP}{d\Omega} d\Omega = R_0 \frac{16\pi^2\sigma^2}{\lambda^2} \qquad \text{Eq. (2)}$$

where P and P_0 are scattered and incident power into the solid angle, Ω and the scattered power is normalized to the incident power. From the kinematical theory of scattering from a multilayer [7,8], with a scattering vector, $q_z = 2\pi/d$=; $q=k_2-k_1$; where **k** is incident and scattered vectors, d= multilayer period (λ/2) and assuming that the amplitude of roughness is sufficiently small when compared to the incident light; $q_z\sigma << 1$, then diffuse scattering is approximately equal to the power spectral density. In the limit that the roughness that is perfectly conformal, the scattering power distribution is then,

$$\frac{1}{P_0}\frac{dP}{d\Omega} = \frac{\pi^2 R_{qz}}{\lambda^4 Sin\theta_1} PSD(\vec{f}) \qquad \text{Eq. (3)}$$

where $R(q_z)$ is the multilayer reflectivity with a reflectivity maximum at the Bragg condition and the scattering is concentrated in the plane of q_z. The rms-roughness can then also be found from integrating the PSD over the spatial frequency range, f,

$$\sigma^2 = 2\pi \int_{f\,\min}^{f\,\max} PSD(f)\, fdf \qquad \text{Eq. (4)}$$

From the reference, Stearns *et. al.* [7], the frequency roughness divisions and origins are given in table 1. For soft x-rays, roughness in the range of .0004–0.1/nm is of particular concern, since it scatters into all angles. Note that, in the small roughness approximation, roughness computed using either method is expected to be the same.

Table 1: Spatial frequency range and multilayer roughness

LSFR	<0.0004/nm	Purely conformal, replicated surface roughness
MSFR	.0004–0.1/nm	Range where top surface of the multilayer is significantly rougher than the substrate due to the additional roughness associated with the growth of the film.
HSFR	> 0.1/nm	Multilayer film growth has a smoothing effect with the damping of the roughness of the substrate

Roughness computed from the fixed angle scatter and angle resolved scatter using the methods described above is plotted in figure 6, against the AFM measured roughness. A fixed uncertainty of 10% is assumed for both measurements. The three sets of data in figure 6 are seen to overlap where the substrate phase roughness heights are large. In the smallest substrate roughness areas, XRS determined roughness is nearly 50% lower than the AFM measured roughness values, and the ARS measurements are a third smaller than the AFM measurements. Essentially we see that the AFM-based roughness measurement overestimates the true EUV roughness of the multilayer film. Observing the PSDs (figure 7), the overestimation may be a result of the AFM noise floor apparent at the highest frequencies. Given current expected specifications of 50 pm for mask RSR, this amount of AFM noise is certainly of concern.

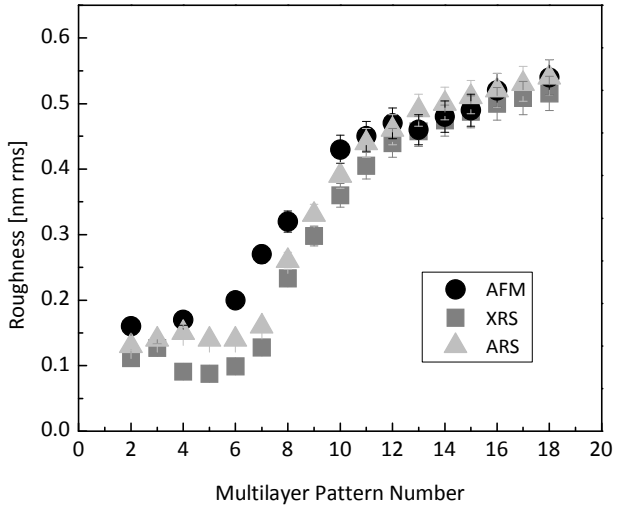

Figure 6: AFM, XRS and ARS measured rms roughnesses are compared. The three sets of data overlap where the substrate phase roughness heights are large, yet they differ by nearly 50% for the low phase roughness mask areas. A fixed uncertainty of 10% is assumed for all sets of data, coming from measurement errors. ARS should give us the most accurate roughness measure and it is still below the AFM based rms roughness.

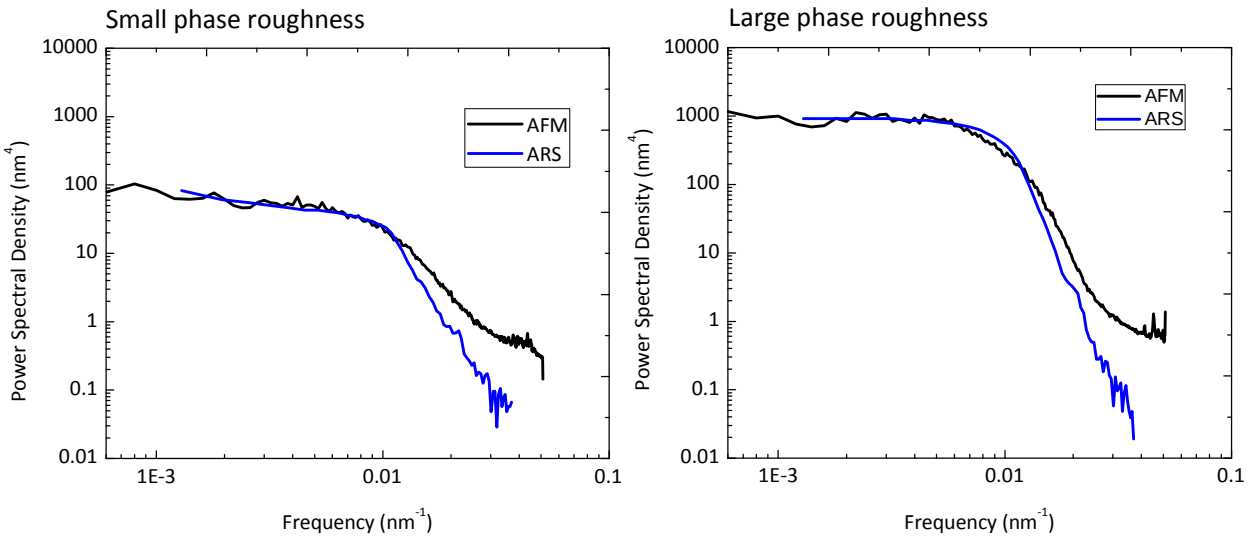

Figure 7: Direct comparison of AFM measured surface PSDs to the PSDs derived from the angle resolved scattering measurement at wavelength. The measurement covers the MSFR for both measurements. In the small roughness content multilayer area, the noise floor of the AFM showing up towards the HSFR has a larger impact.

4. IMAGING MULTILAYER SURFACES WITH THE SEMATECH BERKELEY ACTINIC INSPECTION TOOL (AIT)

The next phase of this study involved the inspection of the various multilayer surfaces with the SEMATECH Berkeley Actinic Inspection Tool (AIT) [2-4]. The AIT is an EUV microscope used for mask imaging at 13.4-nm wavelength. The AIT operates as a high resolution, zoneplate based, EUV microscope designed to emulate EUVL stepper systems. The zoneplate projects a 907x magnified image of the illuminated area on mask onto a back illuminated, 1x1 inch^2, EUV charge coupled device (CCD) camera. Flare in the AIT has been measured in the range of 2–3% [2], the illumination partial coherence is approximately 0.1–0.2. In the AIT's images, the effective pixel size is approximately 15 nm in mask units, significantly oversampling the system's spatial resolution.

Image series were recorded though-focus for four different multilayer surface regions on the mask. Data was collected using a zoneplate objective lens that provides a 4x equivalent NA of 0.3. Analysis was performed to extract the speckle contrast in each image. The details of the measurements and analysis have been discussed previously [9]. Figure 8 gives an example of details from one set of images collected through focus for a single multilayer window. The corresponding speckle contrast is also shown directly below each image in the series. Note that the surface roughness related image variations are strongest before and after focus of the lens.

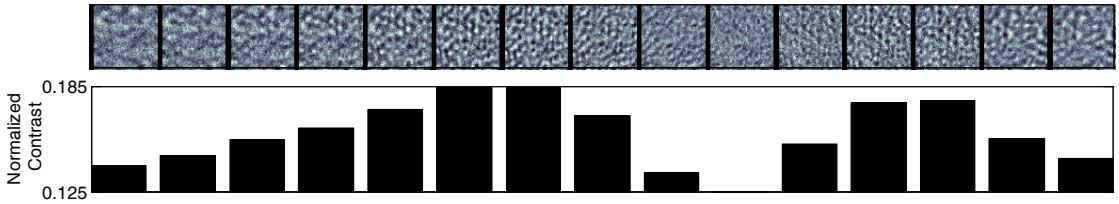

Figure 8: A through focus image series, collected for a single multilayer region using the AIT zoneplate EUV microscope. The corresponding speckle contrast, which is the normalized standard deviation of the image intensity in the detail region, is shown for each image in the series. The minimum speckle contrast occurs in focus, in the 10th image from the left.

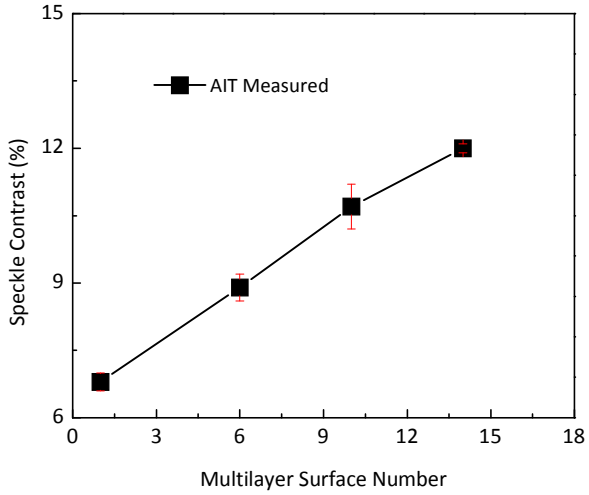

Window	AIT [%]	AFM [nm rms] ±10%
1	6.80 ± 0.2	0.16
6	8.90 ± 0.3	0.20
10	10.7 ± 0.5	0.32
14	12.0 ± 0.1	0.46
18	NA	0.54

Figure 9: The speckle contrast at best focus is shown for four measured regions. The adjacent table provides contrast data as well as the corresponding phase roughness determined from the AFM measurements. Even at the smallest roughness scale, a speckle contrast better than 6% is observed.

Assuming that the intensity variation comes from pure phase roughness, the best focus image coincides with the minimum speckle contrast in the through-focus series. The speckle contrast observed at the best focus of each set of data is plotted against the region number in figure 9 for four measured regions. The adjacent table provides contrast data as well as the corresponding phase roughness determined from the AFM measurements. Even at the smallest roughness scale, a speckle contrast larger than 6% is observed. It should be noted that the relatively high coherence of the AIT's illumination produces larger roughness related contrast variations than may be seen in a typical stepper systems with a greater degree of partial-coherence.

5. MODELING

To investigate the accuracy of the surface characterizations, we try to reproduce the image plane speckle observed in the AIT images by modeling the rms roughness content obtained with the AFM and XRS. AIT imaging characteristics are modeled with a 2-D, scalar, aerial image computation software developed in-house. Scalar modeling and a thin mask approximation is appropriate for the small NAs that are being used here [7]. The mask is modeled as a uniformly reflective surface with pure phase roughness containing a random phase distribution. The phase distribution used in the modeling is synthesized based on the PSDs measured from the AFM images.

Initial calculations completed under the assumption that the AIT images are diffraction limited yielded speckle contrast values that were far from the AIT measured speckle. Subsequent calculations included small aberrations computed for a 1 µm field using raytracing methods tabulated in table in figure 10. Astigmatism and defocus are found to be the dominant field-dependent aberrations. Additionally, a 2.5% speckle pattern attributed to the flare in the AIT is added in quadrature to the modeled speckle contrast at best focus.

The calculated speckle contrast based on the AFM-measured roughness data is compared to the measured speckle, which is shown in figure 10. Although the trend is consistent, AIT measured contrast values are 25% percent higher than the calculated values for much of the range. This difference is observed to be consistent through many simulation sets with small variations in aberration content. When compared to XRS roughness data simulations, the AFM roughness based simulations are closest fit to the AIT measured image intensity variations.

The conclusion of the AFM yielding a better match to the measured speckle data is inconsistent with the fact that the AFM is not a direct measurement of the RSR quantity of interest. The reason for this remains unclear. Moreover, it would be hard to argue that angle resolved EUV scatterometry does not measure the true EUV roughness (RSR) of

concern. The most likely error sources are in the assumptions made in the modeling of the speckle, which depends strongly on the optical aberrations, defocus, coherence, and flare.

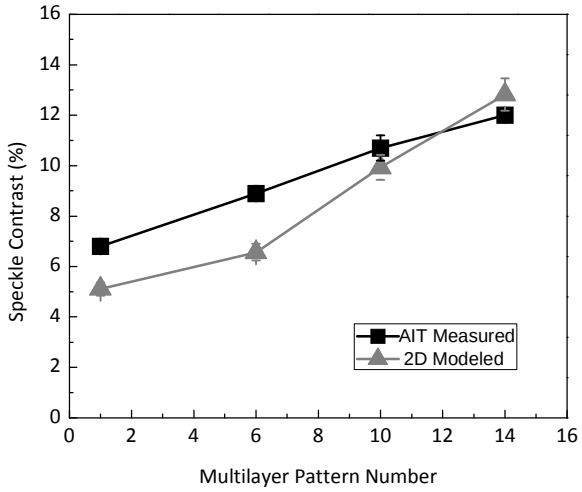

Aberrations	
Defocus	-0.019
Astigmatism 90	0.018
Astigmatism 45	-0.017
Coma X	0.005
Coma Y	0.006
Spherical	-0.0002

2.5% coherent scatter from the optical system

Figure 10: The calculated speckle contrast based on the AFM measured roughness data is compared to the measured speckle. The image contrast measured in the AIT is higher than the calculated values for the low-roughness cases; a crossover point occurs near the high roughness regions.

6. SUMMARY AND FUTURE WORK

In this paper, we try to systematically study the effects of substrate roughness on image plane speckle with the goal of determining adequate metrologies for RSR. Specifically, we considered AFM and X-ray reflectometry, by predicting the speckle based on roughness measured using those techniques and then comparing it to direct AIT speckle measurements. The AFM, XRS, and ARS based measurements of the rms phase roughness are observed to differ in the small roughness range that is characteristic of the EUV mask substrates fabricated at present. Assuming the ARS measurements accurately represent the EUV roughness of concern, we find the AFM overpredicts roughness, and XRS underpredicts roughness. However, the AFM most closely predicts the intensity contrast measured in the AIT, when small amounts of aberrations and flare are added to the calculations. Noting that this is inconsistent with the fact that the AFM cannot measure the true RSR of interest, we conclude that this discrepancy is the result of inaccuracies in the modeling. These results and the importance of this issue to defining workable mask specifications that minimize printed-line LER, warrant continued investigation of this issue. To this end, further evaluations using resist exposures with the SEMATECH Berkeley 0.3 NA MET [10] are being planned.

Acknowledgments

We acknowledge SEMATECH for the support of the SEMATECH Berkeley MET and AIT; in particular, the programmatic support from Warren Montgomery, Bryan Rice, and Stefan Wurm. This work was supported in part by SEMATECH and carried out at Lawrence Berkeley National Laboratory's Advanced Light Source, which is supported by the DOE, Office of Science, and the Basic Energy Sciences under contract no. DE-AC02-05CH11231.

REFERENCES

[1] Patrick P. Naulleau and Simi A. George, Proc. SPIE 7379, 73790O (2009).
[2] K. A. Goldberg, I. Mochi, P. P. Naulleau, H.-S. Han, S. Huh, Proc. SPIE 7122, 71222E-1 (2008).
[3] K. A. Goldberg, I. Mochi, P. Naulleau, T. Liang, P.-Y. Yan, and S. Huh, J. Vac. Sci. Technol. B 27(6), 2916 (2009), and references therein.

[4] The SEMATECH Berkeley Actinic Inspection Tool (AIT), http://ait.lbl.gov
[5] The CXRO Nanowriter Electron-Beam Lithography Lab, http://cxro.lbl.gov/nanofabrication
[6] The CXRO Reflectometer, http://www.cxro.lbl.gov/reflectometer
[7] D. G. Stearns, D. P. Gaines, D. W. Sweeney, and E. M. Gullikson, J. Appl. Phys. 84, 1003 (1998).
[8] D. Stearns and E. Gullikson, Physica B 283, 84-91 (2000).
[9] S. A. George, P. P. Naulleau, F. Salmassi, I. Mochi, E. M. Gullikson, K. A. Goldberg, E. H. Anderson, JVST B 28, (2010)
[10] P. P. Naulleau, C. N. Anderson, L-M Baclea-an, D. Chan, P. E. Denham, S. A. George, K. A. Goldberg, B. Hoef, G. Jones, C. Koh, B. La Fontaine, B. McClinton, R. Miyakawa, W. Montgomery, S. Rekawa, and T. Wallow, Proc. SPIE 7636, 76361J (2010).

DISCLAIMER